Journal of Computational and Applied Research in Mechanical Engineering
jcarme.sru.ac.ir
SRTTU
JCARME
ISSN: 2228-7922

Research paper

Effect of geometrical parameters on fluid film coefficients in tilting pad journal bearing

Harsh Kumar Dixit*and T. C. Gupta

Malaviya National Institute of Technology, Jaipur, Rajasthan, 302017, India

Article info:

Article history:

Received: 10/06/2019
Revised: 21/05/2020
Accepted: 23/05/2020
Online: 26/05/2020

Keywords:

Tilting pad journal bearing,
Hydrodynamic lubrication,
Pad clearance,
Geometric parameters.

***Corresponding author:**
2014rme9552@mnit.ac.in

Abstract

The simplified analytical method has developed to analyze the effect of bearing geometrical parameters, i.e. eccentricity ratio, journal rotation speed, slenderness ratio, bearing radial clearance, pad pivot offset and the number of pads on tilting pad journal bearing (TPJB) properties, i.e. fluid film thickness, fluid film forces and fluid film stiffness and damping coefficients of TPJB. Reynolds equation was solved for each pad to determine fluid film pressure on pads. The infinite short bearing assumption used to determine pressure distribution on pads integrated over the pad surface to find fluid film forces. The pressure distribution and fluid film forces validated with previous researches. Error bars presented to indicate accuracy measurement. The maximum error found was not more than 6 percent corresponding to loaded pads. The percentage error found maximum when the eccentricity ratio is 0.25 while it found a minimum when the eccentricity ratio is 0.62. The Matlab code has been developed for the solution of non-linear equations. Results produced in the form of design curves which compares changes in fluid film properties corresponding to TPJB geometric parameters. The results obtained in this manuscript are applicable in other similar researches to find appropriate and limiting values of fluid film properties at different geometrical and parametric conditions. The generated plots and data are helpful in dynamic analysis to find the value of a specific parameter corresponding to a specific value of fluid film coefficient, which makes an easier selection of suitable numerical integration technique and boundary conditions to avoid non-significant results, which save time and effort in the nonlinear analysis.

1. Introduction

Due to the increasing usage of the high-speed rotating machinery for present-day power demands and industrial usage, the machines have to be operated above critical speeds. The hydrodynamic bearings are proved to be useful to safely pass through these speeds as the rotating components are accelerated [1]. Hydrodynamic bearings are commonly used for applications experiencing higher rated speeds and loads due to high load carrying capacity, high-speed conditions, lower dynamic friction, less power loss, and longer Life. It has some

limitations also, i.e. power loss is high during starting and also high installation & maintenance cost. Tilting pad journal bearings (TPJB's) offer significant advantages over plain cylindrical journal bearings because they provide stable performance for high rotor speed applications. The stable function of TPJB's in high-speed rotating machines (e.g. compressors and turbines) enables their vast uses. Table 1 represents some pros and cons of TPJB over plain journal bearing. Different from fixed geometry fluid film bearings, TPJB's have some accurate pads distributed circumferentially around the bearing.

Each pad can tilt about its pivot to generate a convergent fluid film on the pad surface. A pad cannot support a tilting moment, except for a pad with a flexure pivot. However, more degrees of freedom from the bearing pads motion, i.e., pad tilt motion, makes it difficult in predicting the static and dynamic force performance of TPJBs [2]. Analysis of the behavior of tilting pad bearings is essential for the efficient functioning of rotating machinery. Numerical models exist for the prediction of fluid film behavior, but analytical methods have proved to be much faster than numerical methods [3]. One of the benchmarks and initial works in this field has been presented by Lund [4] by calculating hydrodynamic pressure over each pad by using FDM. The load is determined by the numerical integration of pressure over each pad. The expression of stiffness and damping obtained by fluid film forces for each pad and vector sum of these coefficients is used to find bearing stiffness and damping.

Design curves were used to present the results. Nicholas and Kirk [5] analyzed the effect of pad inertia by adopting Lund's method. He concluded that without pad inertia, there is no effect of cross-coupled stiffness and cross-coupled damping. White et al. [6] used a linear approach to calculate the forces of tilting-pad bearings; that approach consists of the determination of dynamic coefficients.

The nonlinear analysis is used to solve the Reynolds equation. The hydrodynamic forces are found by integrating pressure numerically. The results show that TPJB avoids oil film instability when clearances are small within permissible speed ranges. The results are also validated by performing experiments on the vertical pump. Feng and Chu [7], investigated the effect of geometrical preload in TPJB on vertical rotor stability. Results show that pad preload affects the shaft displacement inside the bearing. Mahfouz and Adams [8] investigated instabilities in three-pads-TPJB supporting the rotor subjected to sub-harmonic and chaotic motion. The numerical approach is used to obtain hydrodynamic pressure and forces.

The results show that pad-preload improves the stability of the system. Okabe and Cavalca [9-10] developed the analytical model to determine the dynamic response of four pads TPJB. The results were compared with an equivalent numerical model. Investigation revealed that the analytical model was up to 100 times faster and that has more precision than an equivalent numerical model. Results indicated that when pad preload increases, fluid film stiffness also increases. Further, the response of the same system was investigated by including the fluid inertia effect.

Fluid film thickness was taken as the function of geometric parameters of TPJB which is a slightly improved version of film thickness adopted in the previous method [9]. Results show that the effect of fluid inertia is very small in the order of 2%. It generates more hydrodynamic load but does not significantly alter TPJB stiffness and damping [10]. Luneno et al. [11, 12] simulated a vertical rotor-bearings system supported by a combined tilting pad journal and thrust bearing. The analytical approach is used to derive the bearing model. The analytical model is validated by the experimental setup. Investigation revealed that combined tilting pad journal and thrust bearing influences fundamental natural frequencies; neglecting the inclusion of these bearings in the system, the analysis produces significant errors.

Nasselqvist et al. [13] used time step polynomials to calculate TPJB's parameters at given eccentricities and load angles. The test rig was used to compare results. Due to difficulties in calculations, there is a small deviation observed between analytical and experimental results. Synnegard et al. [14, 15] analyzed the unbalance response of flexible rotor supported by 4-pad tilting pad journal bearings at the end.

Table 1. Pros and cons of TPJB.

No	Pros	Cons
1	The self-adjustment of the pads causes the optimal oil wedge at each loaded pad to make TPJB inherently stable and useful in high-speed applications.	The additional degrees of freedom of pads make more complex geometry as well as difficulty in analysis; it is expensive to fabricate and require careful design procedures.
2.	The rocking characteristic of the pads in TPJB enables the journal motion causing less magnitude of the destabilizing, cross-coupled stiffness, and damping coefficients, which are the main sources of instabilities in machinery supported on fixed geometry journal bearings.	The pad clearances and assembly clearance are different so operational clearances are difficult to determine. that increases complications in design procedure and difficulties arise to provide mechanical preload. At low preload, there is a risk of the flutter of unloaded pads, also pivoting material causes friction problems and sudden changes in temperature in fluid film properties.
3.	TPJB has various pads that make short bearing segments and cold oil supply at each of the leading edges on pads reduces the bearing temperature.	High temperatures in the pads correspond to low fluid film thicknesses cause large thermal deformations in the pads.
4.	Flexibility for designing various segments i.e. pad size, pivot angle, pad pivot offset, fluid supply locations, etc. makes it applicable to a wide range of design parameters.	Poor response to external excitations, such as synchronous dynamic force resulting from rotor unbalance; also it provides less damping at critical speed and also causes large power loss at high speeds.

The simulated results were compared with experimental results. It is observed that cross-coupled stiffness and damping coefficients influence the rotor-bearing system response by increasing higher frequency components. The angular shaft position influences cross-coupling coefficients and direct and cross-coupled stiffness. Khosravian and Ghatreh [16] Used analytical and experimental techniques to evaluate stiffness and damping factors for four pad TPJB and analyzed changes in those factors with excitation frequencies which depends on TPJB operating situations. The analytical technique was based on a three-dimensional model of tilting-pad journal bearings while an experiment was conducted on Journal bearing dynamic test rig to collect data.

The power spectral density method has been used to evaluate the bearing stiffness and damping factor. Reduction in stiffness and damping coefficients is observed with an increment of excitation frequencies at TPJB horizontal and vertical directions. Chasalevris [17] presented a closed-form analytical solution of the Reynolds equation for finite length three-lobe bearing that can be easily integrated into rotor-dynamic algorithms. That claims to be reliable and have low computational cost. Change in stiffness and damping coefficients of three-lobe bearing is analyzed for different values of preloads, slenderness ratios. Results were presented as a function of the Sommerfeld number. Sharabiani and Ahmadian [18] proposed a nonlinear model providing a fast computational tool to investigate the nonlinear behavior of TPJB.

The least mean square technique in the time domain is used to identify fluid film coefficients of the nonlinear model. The dominant terms in nonlinear oil film forces are selected by the subset selection method. The proposed nonlinear model of reduced-order is a suitable alternative for the direct integration method of the Reynolds equation. The numerically simulated data have been evaluated according to unbalance force which used to set up a system of linear equations to find the nonlinear coefficients. Dang et al. [19] calculated characteristics of five pad TPJB having non-nominal geometry with different geometrical preload factor for each pad, using hydrodynamic lubrication theory as a function of loading condition.

The obtained results are compared with experimental measurements. A linear estimator is derived based on the least square estimation by which all dynamic coefficients can be calculated through one operation. Due to the asymmetric geometry of TPJB, the clearance profile of the test bearing is very different from that of symmetric one, in both nominal and non-nominal bearing configuration.

The measured direct stiffness and damping coefficients were found smaller than the calculated ones. Results indicated the significance of cross-coupling dynamic coefficients during the evaluation of the dynamic characteristics of non-ideal TPJB. Jin et al. [20, 21] demonstrated the modified database method to rapidly determine fluid film forces of four pads. The nonlinear fluid film force database for

a single pad is constructed by solving a hydrodynamic model having five equivalent state variables of the journal. The combined liner and parabolic interpolation polynomial based on the database are determined to calculate nonlinear forces of the tilting pad. Results show the negligible effect of temperature on the dynamics of TPJB; also they investigated the effect of design parameters on the minimum fluid film thickness of four pads water-lubricated TPJB with and without static loads. Results show that fluid film forces increase when there is an increment in preload factors and pivot offset, also fluid film forces decrease with increment in clearance ratio and fluid temperature.

The minimum fluid film thickness gets improved by increasing slenderness ratios, pad arc angles, and decreasing preload factors. The optimum pad pivot offset should be smaller than 50%, to maximize fluid film thickness. The four pads and five pads TPJB without static load and three pads and four pads TPJB with static load leads to optimal fluid film thickness also four pads TPJB shows similar amplitudes in horizontal and vertical directions. Ciulli et al. [22, 23] investigated the characteristics of four pads TPJB by the novel experimental setup. The test set up can investigate large size TPJB with different diameters at high peripheral speeds and different loads. The results showed unexpected behaviors at the transition from laminar to turbulent flow regime; during experimental identification of dynamic bearing coefficients of TPJB were considered linear.

A quasi-static procedure was used in a novel way and linear displacement range was used to estimate TPJB stiffness. The experimental nonlinear results were replicated by simple nonlinear models for the analysis. The results indicated equal direct and cross-coupled stiffness coefficients for four pads TPJB. Silva and Nicoletti [24] performed the stochastic analysis to find the probability of failure in 4 pads TPJB in which clearance at each pad is an independent random variable as it varies between the minimum and maximum values. The process of choosing the combination of values of the assembled clearance was based on the Monte Carlo method where the values are randomly distributed in the working range according to a probability density function. Results indicate that the asymmetry of the bearings does not affect dynamic coefficients significantly.

The determined cross-coupled coefficients were small. Andres et al. [25] investigated the effect of lubricant starvation on four pads TPJB. Starvation occurs on unloaded pads but depends on supplied flow rate; if it moves towards loaded pads, it increases journal eccentricity and changes dynamic force coefficients of the whole bearing which causes reduction in system natural frequencies and damping ratios particularly in lower modes. Barsanti et al. [26, 27] proposed a systematic error method that affects the computation of dynamic stiffness and damping coefficients of five pads TPJB.

The coefficients were computed by data acquired during tests with linear independent excitations. Results show that errors associate with each coefficient is of the same magnitude as the order of random uncertainties. They described a new statistical method for the determination of dynamic coefficients of five pads TPJB by linear coefficient identification procedure, which is based on dynamic measurement of forces, accelerations, and relative displacements of rotor and bearing. The least-square minimization technique is used to determine dynamic coefficients. Ito et al. [28] used the design of experiments to study the influence on the dynamic response of the rotor-TPJB system hence it is capable of evaluating the influence of each of the studied parameters and effect of possible coupling between them. The finite volume method was applied to TPJB to determine synchronous stiffness and damping coefficients. Computational analysis was carried out by integration using commercial design software and numerical code was implanted in Matlab to simulate the rotor-dynamic phenomenon. The results indicated that contributions of geometric parameters are different and the pivot offset has greater contributions to the system's response.

Although there is much development work conducted on TPJB bearing, yet the degree of maturity for predicting the overall behavior of the system, has been a somewhat open question. Due to complex calculations and the requirement of high computation cost, limited work has been conducted to understand the dynamic behavior of TPJB. Rigorous calculations are required due to the nonlinear properties of the fluid film; standard analytical expressions do not exist. The

numerical methods adopted to solve the Reynolds equation at each time step to update the stiffness and damping coefficients cause an increase in simulation time so that parametric studies become rigorous. So in the present paper, instead of the numerical method, the simplified analytical method is used to perform the effect of TPJB geometric parameters such as journal eccentricities, rotational speeds, radial clearances, slenderness (L/D) ratios, pivot offset and number of pads, on TPJB's fluid film properties. Matlab code has been developed to solve nonlinear equations to generate data represented in the form of design curves.

The contribution of present research work is to find the trends and values of fluid film properties at different geometrical and operating parameters. These findings are considered as a platform to determine the critical and/or threshold value of fluid film properties, and thus this work provides sufficient data for designing TPJB at a lesser computational cost. The data can also be used to identify applicable initial, threshold, or boundary value for numerical integration to get a dynamic response.

The results obtained in this manuscript are applicable in other similar researches to find appropriate and limiting values of fluid film forces, stiffness, and damping coefficients at different geometric and parametric conditions. The generated plots and data are helpful in dynamic analysis to find trends and value of a specific parameter corresponding to the specific value of the fluid film coefficient, which makes the selection of suitable numerical integration techniques and boundary conditions to avoid non-significant results. This saves time and effort, particularly in the nonlinear analysis; also it is applicable to find dimension and specification of the geometrical parameter to design TPJB within the specific range of operations.

2. Mathematical model

The hydrodynamic action in fluid film bearing is due to the interaction of fluid and solid structure. The lateral stiffness and damping coefficients find out by linearization of interaction and then perturbed at 2-orthogonal directions. Fig.1(a) indicates a 3D model of 4-pad tilting pad bearing represents parts of bearing. Fig. 1(b) represents a vertical rotor supported by two TPJB's situated at upper and lower ends. The equation of motion represented as:

$$M_B\ddot{U}_B + D_B\dot{U}_B + S_BU_B = F_h(t) \qquad (1)$$

Here S_B is the stiffness matrix, D_B is the damping matrix, M_B is the fluid inertia matrix, and $F_h(t)$are the fluid film forces which are functions of displacements and velocities. Fig. 2. represents geometrical parameters of a TPJB, it contains 4-pads, placed symmetrically inside bearing. Table 2 represents the values of geometrical parameters and their corresponding symbols used for analysis. Fig. 3. represents the steps involved in the analysis. To model hydrodynamic bearing. The initial step is to develop an equation for the bearing fluid film thickness H on each pad, which has to consider the displacement of the journal center about bearing center, preload coefficients, and pivot location (angle).

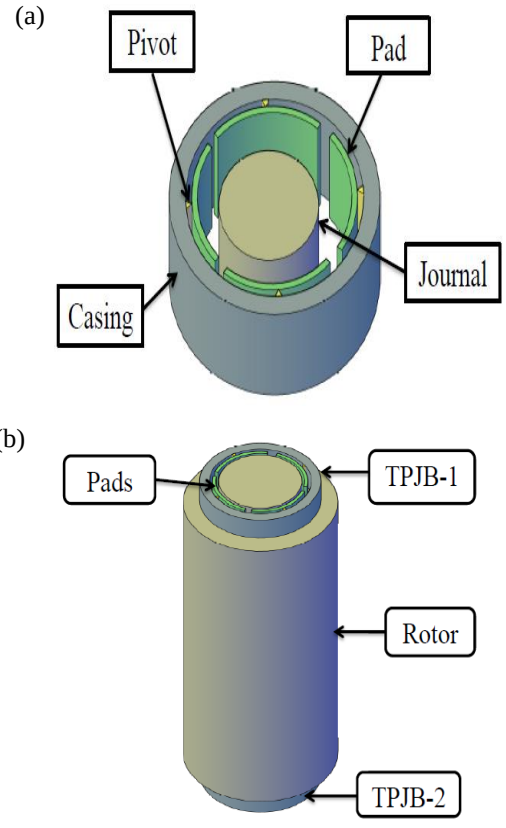

Fig. 1. (a) Tilting pad journal bearing representing various parts**,** (b) vertical rotor supported by TPJB's at upper and lower ends.

Table 2. Geometrical details of TPJB.

No	Symbol	Name	Value	Unit
1	C_r	Bearing radial clearance	125e-6	Meters
2	N	Journal revolution	2500	Rpm
3	D_j	Journal diameter	50e-3	Meters
4	R_0	Pivot distance from bearing center	25.1e-3	Meters
5	T_p	Pad thickness	0.0	Meters
6	L	Bearing length	25e-3	Meters
7	m	Pad preload	0.1	Unit-less
8	ϕ_{01}	Pad-1 pivoting angle	45	Degrees
9	μ	Fluid dynamic viscosity	8.95e-4	Pa*sec
10	Φ_l	Pad-1 leading edge angle	05	Degrees
11	Φ_t	Pad-1 trailing edge angle	85	Degrees
12	N_p	Number of pads	04	Unit-less

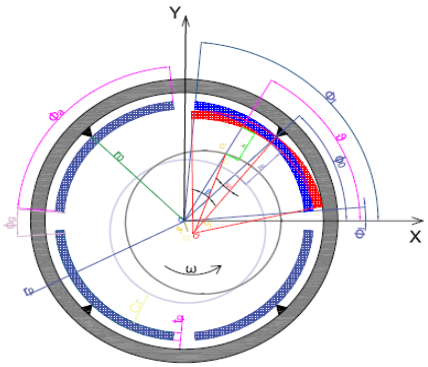

Fig. 2. Geometrical parameters of TPJB.

Santos et al. [29] derived the expression of film thickness on the pad. The modified equation of fluid film thickness has determined as:

$$H = C_r\text{-}(X - A)\cos\vartheta_b\text{-}(Y - B).\sin\vartheta_b \quad (2)$$

Here C_r is bearing radial clearance, X is the displacement of the journal along bearing X-axis Y is the displacement of the journal along bearing Y-axis, ϑ_b is bearing circumferential coordinate.
pivot distance from pad curvature center (X_0, Y_0) and pad pivot angle in bearing coordinate system $(\emptyset_0)$ and can be represented as:

$A = A_{p1} - A_{p2}$ Were $A_{p1} = C_r.\psi.Y_0$ and $A_{p2} = C_r.m.\cos(\emptyset_0)$ $B = B_{p1} - B_{p2}$
$B_{p1} = C_r.\psi.X_0$ and $B_{p2} = C_r.m.\sin(\emptyset_0)$
$X_0 = R_0\cos(\emptyset_0)$, $Y_0 = R_0\sin(\emptyset_0)$

By doing non-dimensioning of above-mentioned variables, Eq. (2) in the non-dimensional form written as:

$$h = 1\text{-}(x - a)\cos\vartheta_b\text{-}(y - b).\sin\vartheta_b \quad (3)$$

Here:

$h = \frac{H}{C_r}$, $x_p = x - a$, $y_p = y - b$, $a = (\psi.y_0) - m.\cos(\emptyset_0), b = (\psi.x_0) - m.\sin(\emptyset_0)$

The hydrodynamic pressure P determined by solving the Reynolds equation by taking infinite short bearing assumption. The generalized expression of the Reynolds equation is given as [30]:

$$\frac{1}{{R_b}^2}\frac{\partial}{\partial\vartheta_b}\left(\frac{H^3}{\mu}.\frac{\partial P}{\partial\vartheta_b}\right) + \frac{\partial}{\partial Z}\left(\frac{H^3}{\mu}.\frac{\partial P}{\partial Z}\right) = 6\left(\omega.\frac{\partial H}{\partial\vartheta_b} + 2\frac{dH}{dt}\right) \quad (4)$$

Here, Z is axial coordinate, R_b is bearing radius, ϑ_b is circumferential coordinate, μ is the dynamic viscosity of the fluid, H is dimensional fluid film thickness, P is dimensional pressure, and t is the time. Apply the short bearing assumption by neglecting pressure gradient on circumferential direction Eq. (4) becomes:

$$\frac{\partial}{\partial Z}\left(\frac{H^3}{\mu}.\frac{\partial P}{\partial Z}\right) = 6\left(\omega.\frac{\partial H}{\partial \vartheta_b} + 2\frac{dH}{dt}\right) \quad (5)$$

By integrating this equation and applying boundary conditions as:

$$Z = -\frac{L}{2}, P = 0 \; ; \; Z = \frac{L}{2}, P = 0$$

Here L is the axial length of TPJB and Z is an axial coordinate of TPJB.
The expression of dimensional pressure distribution at each pad is given by:

$$P = \frac{3\mu}{H^3}\left(Z^2 - \frac{L^2}{4}\right)[\{\omega(X-A)\,2\dot{Y}\}\sin\vartheta_b - \{\omega(Y-B) + 2\dot{X}\}]\cos\vartheta_b \quad (6)$$

Here $\dot{X}$ is the velocity of the journal along bearing X-axis, $\dot{Y}$ is the velocity of the journal along bearing Y-axis and ω is the angular velocity of the journal. In Non-dimensional Form:

$$p = \frac{P}{P_0} \quad \text{Where } P_0 = 6\mu\omega\left(\frac{R}{C}\right)^2$$

$$p = \frac{1}{2}\left(\frac{L}{D}\right)^2\left(\frac{4z^2-1}{h^3}\right)\left[\begin{matrix}\{(x-a) - 2\dot{y}\}\sin\vartheta_b - \\ \{(y-b) + 2\dot{x}\}\cos\vartheta_b\end{matrix}\right] \quad (7)$$

Here:

$$x = \frac{X}{C_r}, y = \frac{Y}{C_r}\; z = \frac{Z}{L}, \dot{x} = \frac{\dot{X}}{C_r\omega}, \dot{y} = \frac{\dot{Y}}{C_r\omega}$$

Above mentioned terms are non-dimensional displacements and velocities. The reaction fluid film forces of the pad are calculated by the integration of pressure on pads. These forces are functions of the journal displacement and the journal center velocity at that instant along X-direction and Y-direction. The initial position of the journal inside the bearing depends on the journal's rotational speed. The differential contact area ($dA = R_b.L.d\vartheta.dZ$) is considered in the integration. Here R_b is the TPJB assembly radius.

$$F_X = \int_{\vartheta_1}^{\vartheta_2}\int_{-\frac{L}{2}}^{\frac{L}{2}} P.R_b\;\cos\vartheta_b\;d\vartheta_b.dZ$$

$$F_Y = \int_{\vartheta_1}^{\vartheta_2}\int_{-\frac{L}{2}}^{\frac{L}{2}} P.R_b\;\sin\vartheta_b\;d\vartheta_b.dZ$$

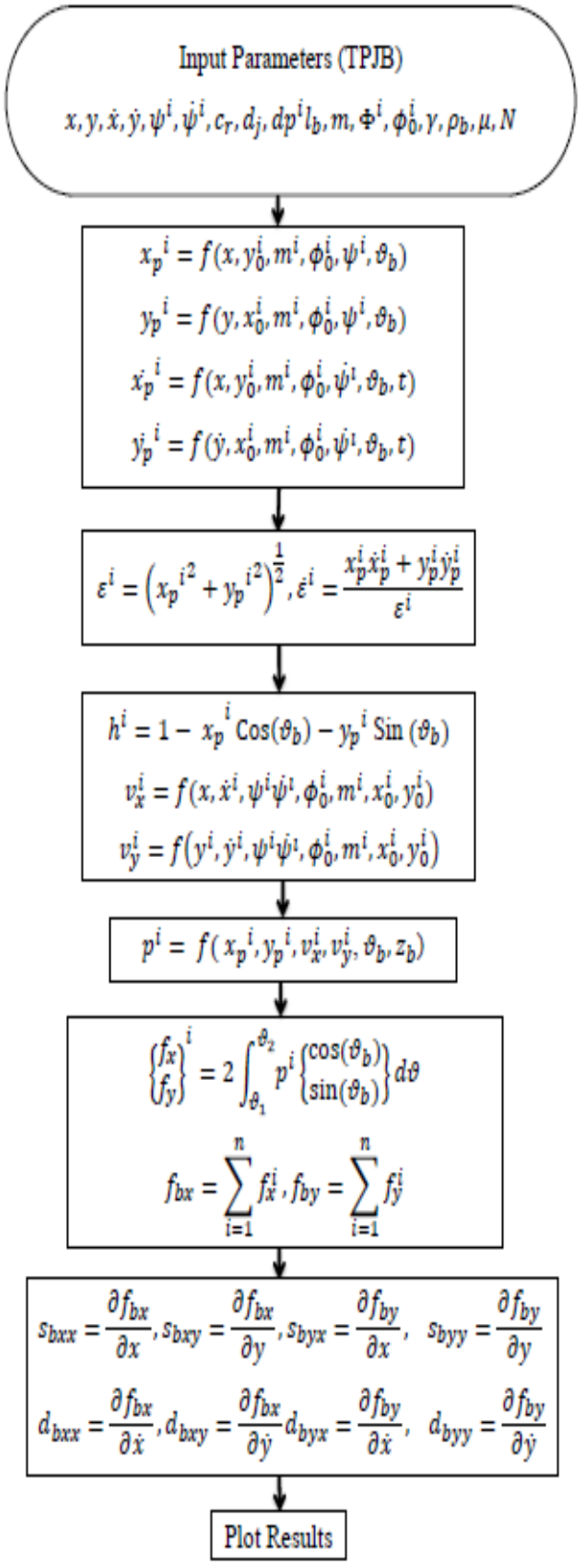

Fig. 3. Flow chart for determination of fluid film coefficients.

In non-dimensional form:

$$\begin{Bmatrix} f_x \\ f_y \end{Bmatrix} = \int_{\vartheta_1}^{\vartheta_2} \int_{-\frac{1}{2}}^{\frac{1}{2}} p.r_b \begin{Bmatrix} \cos\vartheta_b \\ \sin\vartheta_b \end{Bmatrix} d\vartheta \quad (8)$$

There are some assumptions as fluid is not compressible, and the viscosity is assumed to be constant across the fluid. Half sommerfeld solution applied and cavitation effect has neglected, considering null pressure for negative values of pressure distribution, for a single pad integral function G can be determined as:

$$G = \int_{\vartheta_1}^{\vartheta_2} \frac{d\vartheta_b}{1-(x-a)\cos\vartheta-(y-b)\sin\vartheta} \quad (9)$$

The integrals I_1 , I_2 and I_3 determined as:

$$I_1 = \frac{1}{2}\frac{\partial^2 G}{\partial x \partial y} , I_2 = \frac{1}{2}\frac{\partial^2 G}{\partial x^2} , I_3 = \frac{1}{2}\frac{\partial^2 G}{\partial y^2} \quad (10)$$

Here:

$$I_1 = \int_{\vartheta_1}^{\vartheta_2} \frac{\sin\vartheta_b \cos\vartheta_b}{1-(x-a)\cos\vartheta_b-(y-b)\sin\vartheta_b} d\vartheta_b \quad (11)$$

$$I_2 = \int_{\vartheta_1}^{\vartheta_2} \frac{\cos^2\vartheta_b}{1-(x-a)\cos\vartheta_b-(y-b)\sin\vartheta_b} d\vartheta_b \quad (12)$$

$$I_3 = \int_{\vartheta_1}^{\vartheta_2} \frac{\sin^2\vartheta_b}{1-(x-a)\cos\vartheta_b-(y-b)\sin\vartheta_b} d\vartheta_b \quad (13)$$

The expression of non-dimensional hydrodynamic fluid film force on each pad has determined as:

$$\begin{Bmatrix} f_x \\ f_y \end{Bmatrix} = -kt \begin{bmatrix} I_{f1}.I_1 - I_{f2}.I_2 \\ I_{f1}.I_3 - I_{f2}.I_1 \end{bmatrix} \quad (14)$$

Here:

$$kt = \frac{1}{3}\left(\frac{L}{D}\right)^2 r_b$$
$$I_{f1} = \{(x-a) - 2\dot{y}\}$$
$$I_{f2} = \{(y-b) + 2\dot{x}\}$$

Negative direction indicates that force is acting towards the journal from the fluid film. The dimensional fluid film force at each pad represented as:

$$\begin{Bmatrix} F_X \\ F_Y \end{Bmatrix} = \mu\omega \left(\frac{R_b}{C_r}\right)^2 \left(\frac{L}{D}\right)^2 R_b\, L \begin{Bmatrix} f_x \\ f_y \end{Bmatrix} \quad (15)$$

The fluid film forces of the whole bearing can be obtained by vector summation of forces from each pad to journal along bearing axis as:

$$F_{bX} = \sum_{i=1}^{n} F_X^i \ , F_{bY} = \sum_{i=1}^{n} F_Y^i \quad (16)$$

Here n is the number of pads in TPJB. Stiffness and damping coefficients of bearing determined by differentiating force expression to instantaneous journal displacements and velocities as:

$$S_{bXX} = \frac{\partial F_{bX}}{\partial X}, S_{bXY} = \frac{\partial F_{bX}}{\partial Y}$$
$$S_{bYX} = \frac{\partial F_{bY}}{\partial X}, S_{bYY} = \frac{\partial F_{bY}}{\partial Y}$$
$$D_{bXX} = \frac{\partial F_{bX}}{\partial \dot{X}}, D_{bXY} = \frac{\partial F_{bX}}{\partial \dot{Y}}$$
$$D_{bYX} = \frac{\partial F_{bY}}{\partial \dot{X}}, D_{bYY} = \frac{\partial F_{bY}}{\partial \dot{Y}}$$

Here:
S_{bXX} , S_{bYY} are direct stiffness coefficients and S_{bXY} , S_{bYX} are cross-coupled stiffness coefficients.
D_{bXX} , D_{bYY} are direct damping coefficients and D_{bXY} , D_{bYX} are cross-coupled damping coefficients.

3. Results and discussion

Fig. 4(a) represents a comparison between non-dimensional pressure distribution at different pads by mentioned analytical method (continuous curve) and the variable separation method mentioned (dotted curve) by wang et al. [31] The result has shown good agreement with each other. As the journal center position is at the fourth quadrant, the highest non-dimensional fluid film pressure was observed pad-4 by the proposed method having value 0.4078 at the axially mid part of the bearing while the lowest value of pressure is 0.0381 obtained at pad-2. Both lowest and highest non-dimensional pressures obtained at the axially mid part of the bearing. That indicates the proposed method covers a large number of pressure variations on pads.

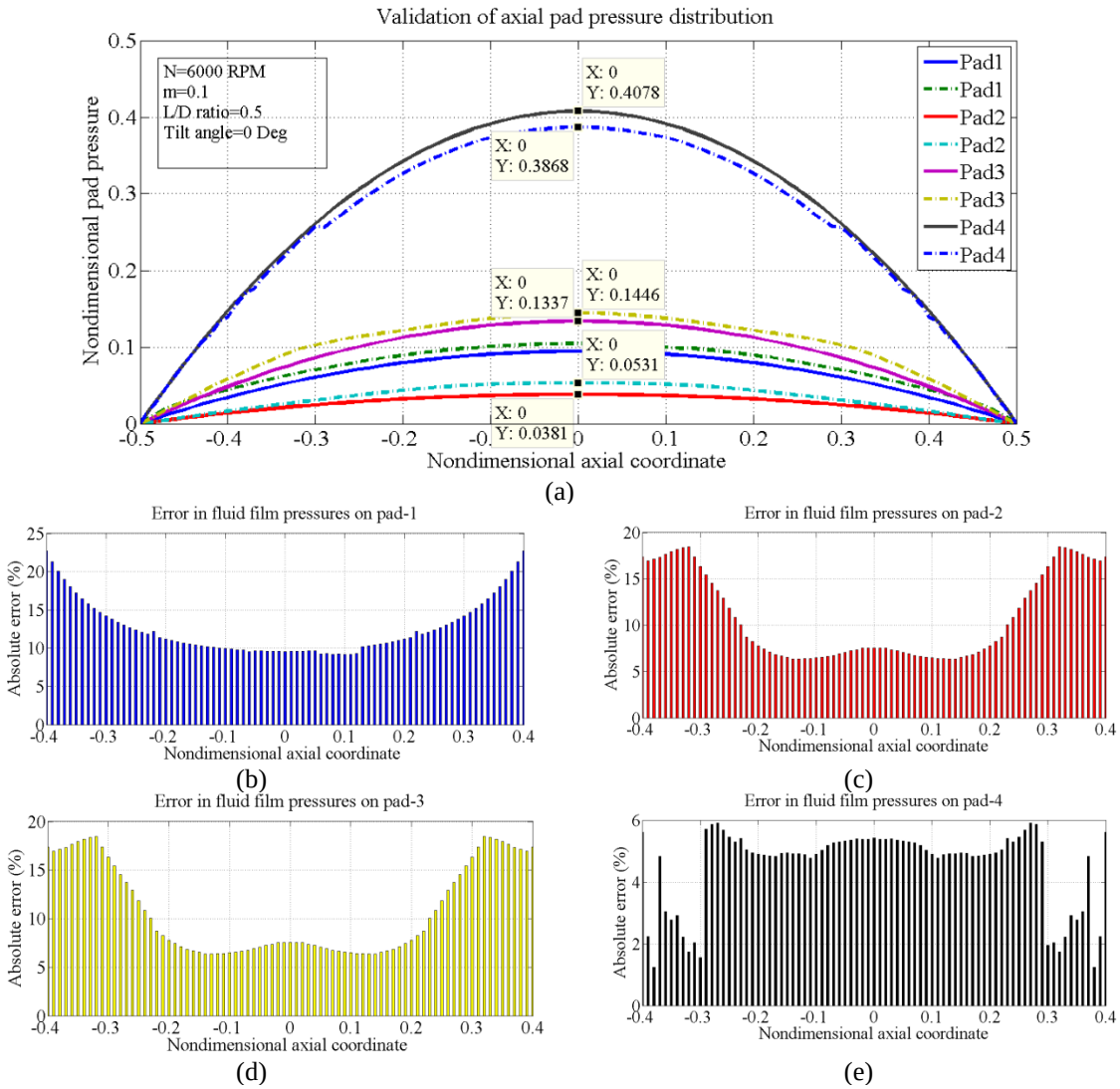

Fig. 4. (a) Non-dimensional axial pressure distribution on pads (continuous line represents the current method while the dotted line represents the method adopted by wang et al. [31]), (b) absolute percentage error in pressure on pad-1 corresponding to non-dimensional axial coordinate, (c) absolute percentage error in pressure on pad-2 corresponding to non-dimensional axial coordinate, (d) absolute percentage error in pressure on pad-3 corresponding to non-dimensional axial coordinate, (e) absolute percentage error in pressure on pad-4 corresponding to non-dimensional axial coordinate.

Fig. 4(b-d) represents the percentage of absolute errors in non-dimensional pressure calculated by the proposed method and method adopted by wang et al. [31] on different pads. Observations indicate that percentage errors are higher at corners of pad-1, pad-2, and pad-3 while at pad-4, errors are higher at the axially middle part of the pad yet the amount of error is less than 6 %. As atmospheric pressure has taken as datum pressure, at the end of pads pressures observed zero.

Fig. 5(a) represents the change in non-dimensional fluid film forces corresponding to the journal eccentricity ratios by the proposed method and method adopted by Lu et al. [32]. These values are also showing agreement with each other. Both methods show identical values of non-dimensional fluid film force when non-dimensional eccentricities are 0.47, 0.58, and 0.7. At zero journal eccentricity ratio, there will be some fluid film force acting towards the journal because of the dead weight of the journal.

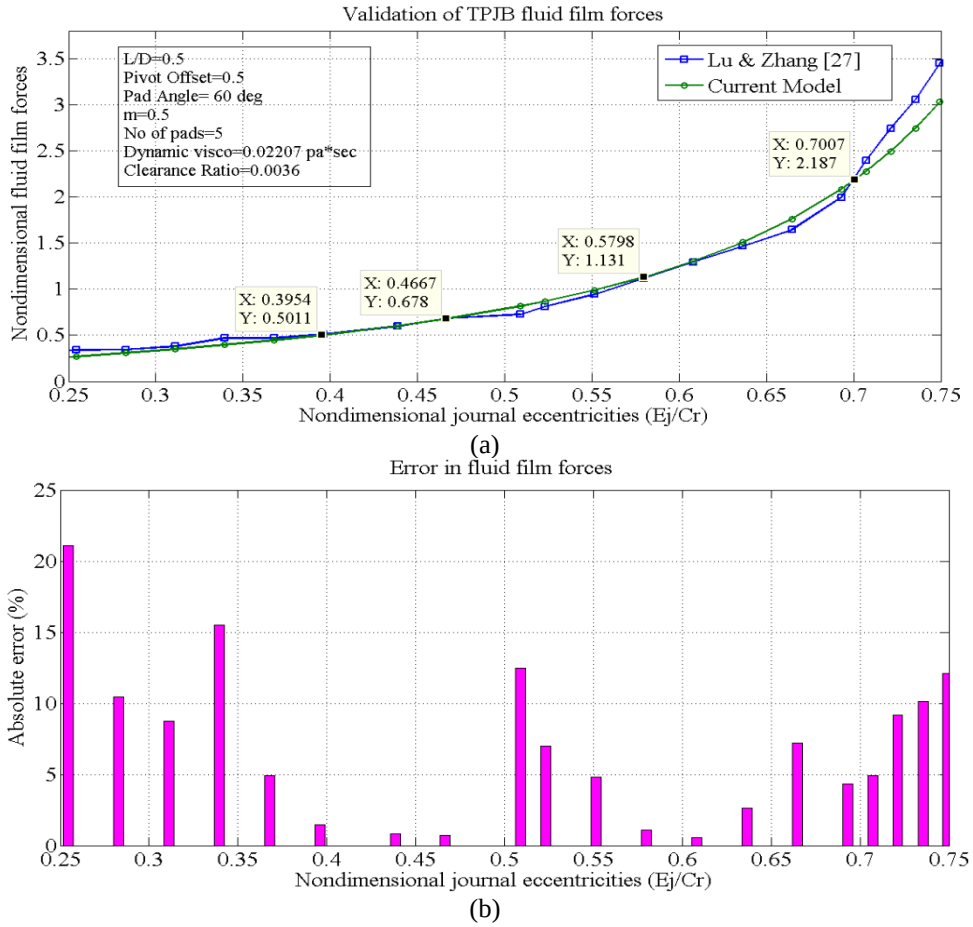

Fig. 5. (a) Change in non-dimensional fluid film forces corresponding to journal eccentricity ratios by current method represents in green colour while the change in non-dimensional fluid film forces corresponding to journal eccentricity ratios in represents method adopted by Lu et al. [32] denoted by blue colour, (b) absolute percentage error in TPJB forces corresponding to non- dimensional journal eccentricities.

Fig. 5(b) represents the percentage of absolute errors in non-dimensional fluid film forces calculated by the proposed method and method adopted by Lu & Zhang [27]. The percentage error found maximum when the eccentricity ratio is 0.25 while it found a minimum when the eccentricity ratio is 0.62. The errors increase at lower eccentricity ratios also it increased when eccentricity ratios higher than 0.75. It should be noted that most of the journals working safely about 0.6 eccentricity ratio.

3.1. Effect of journal eccentricity

Journal eccentricity is the distance between the bearing center and the journal center. As TPJB's included the number of arcuate pads, the bearing center is the intersection point of pad pivot lines. The attitude angle is an important parameter that defines the location of the journal center inside TPJB. Fig. 6 (a) represents the change in the non-dimensional fluid film thickness on all four pads corresponding to non-dimensional journal eccentricities. The figure indicates that fluid film thickness decreases nonlinearly when the eccentricity ratio increases. Higher values of fluid film thickness observed on pad-3 while lower values of fluid film thickness observed on pad-1. That is because both pads lie opposite sides of the bearing prove the accuracy of the proposed analysis in practical situations. The values of non-dimensional fluid film thickness on each pad corresponding to eccentricity ratios of 0.1 to 0.5 have presented in the mentioned figure. The values of non- dimensional fluid film thickness should remain under unity to obtain correct results.

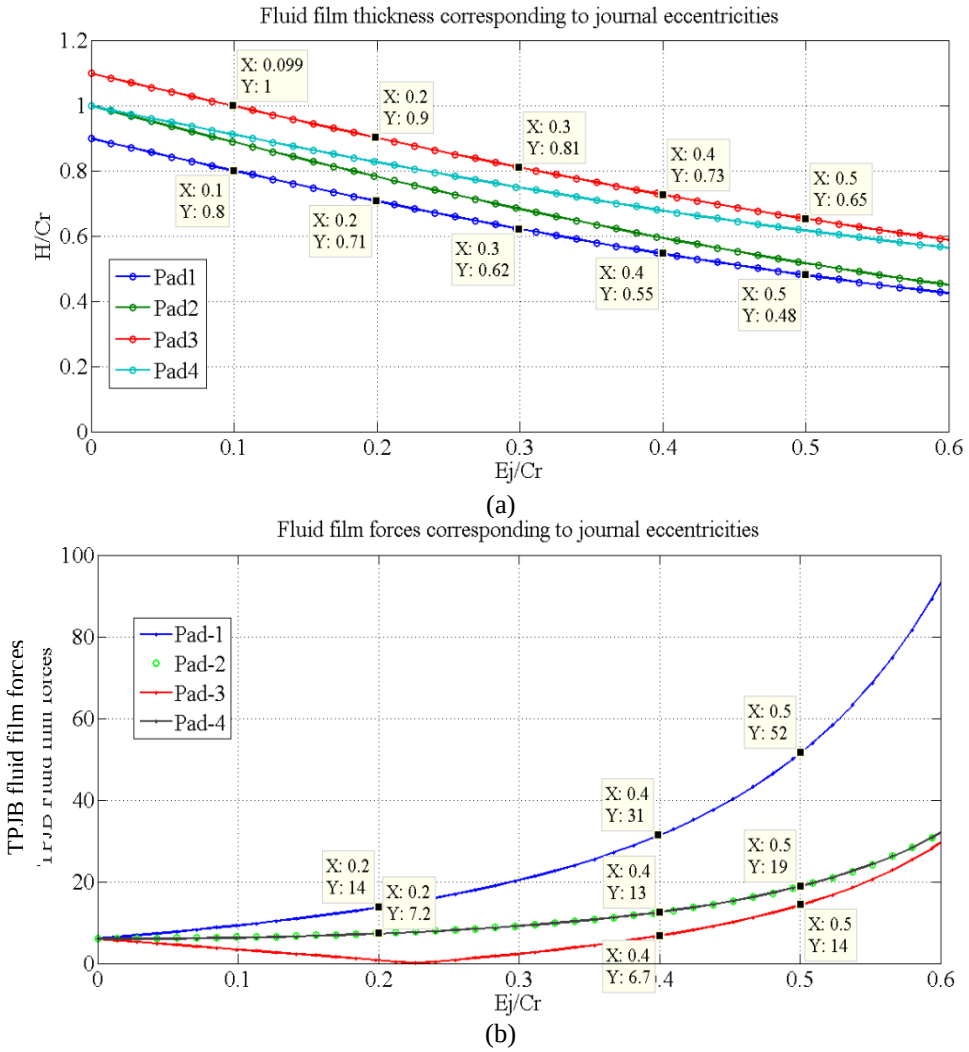

Fig. 6. Change in fluid film properties corresponding to non-dimensional journal eccentricities, (a) non-dimensional fluid film thickness on pads. (b) non-dimensional fluid film forces on pads.

Fig. 6(b) indicates that higher fluid film forces observed on pad-1 because oil thickness is minimum on pad-1, as mentioned in Fig. 6(b) and lower fluid film force on pad-3 because fluid film thickness is high as per Fig. 6 (a). The minimum fluid film thickness observed at pad-3 when the eccentricity ratio is 0.23. Forces on pad-2 and
pad-4 are showing identical values corresponding to eccentricity ratios. Values of non-dimensional fluid film forces on each pad corresponding to journal eccentricity ratios of 0.2, 0.4, and 0.5 mentioned inside Fig. 6(b). Fig. 7(a) represents the change in non-dimensional stiffness coefficients of whole TPJB corresponding to non-dimensional journal eccentricities. The values of direct stiffness coefficients observed higher than cross-coupled stiffness coefficients and the difference increases with journal eccentricity ratios. That result shows an agreement with previous research [14], also at lower eccentricities, cross-coupled stiffness is not much significant but, as eccentricity increases, they become significant.
The values non-dimensional of direct and cross-coupled stiffness corresponding to journal eccentricity ratios of 0.2, 0.3, 0.4, 0.5, and 0.6 are shown in Fig. 7(a) by data strips. Fig. 7(b) represents the change in non-dimensional damping coefficients of whole TPJB corresponding to non-dimensional journal eccentricities.

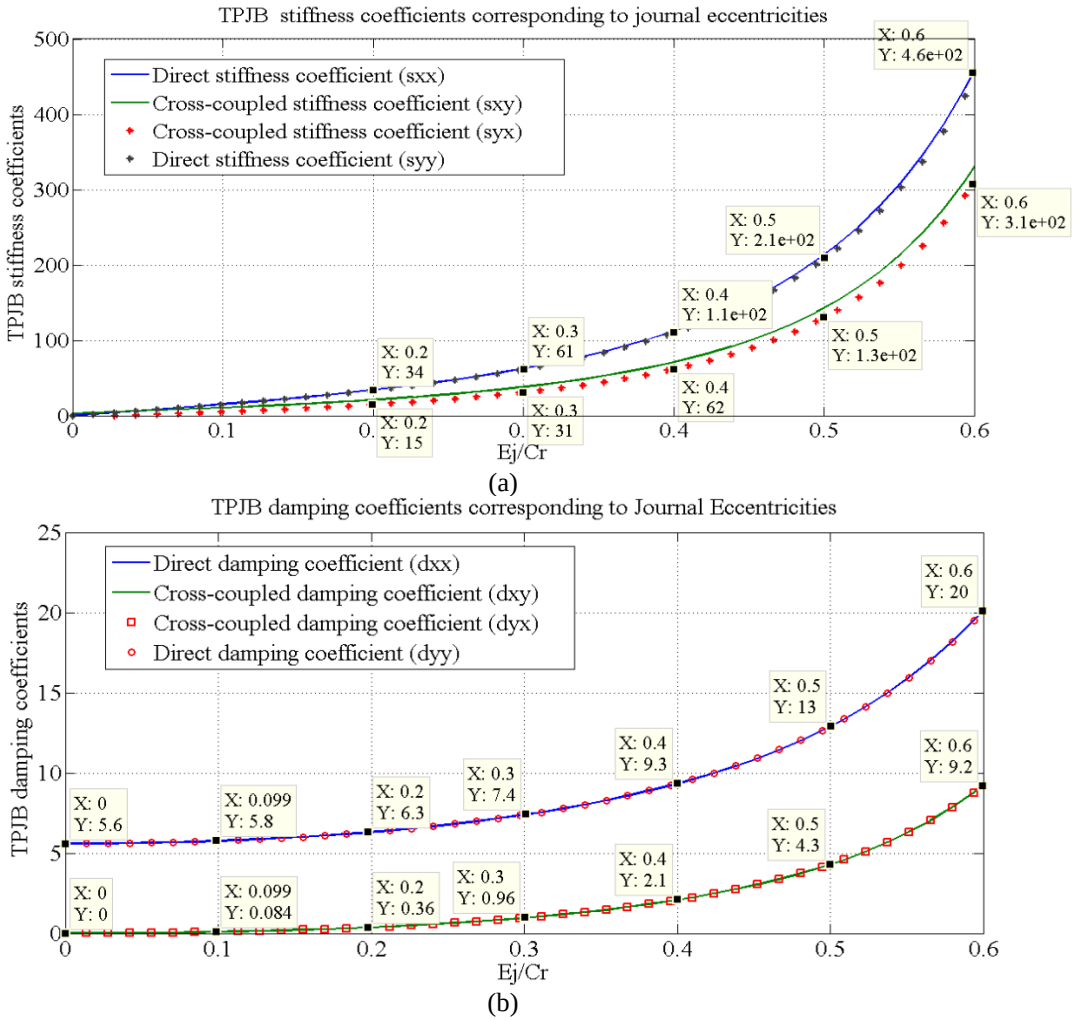

Fig. 7. Change in fluid film properties corresponding to journal eccentricity ratios, (a) non-dimensional fluid film stiffness coefficients of TPJB, (b) TPJB non-dimensional fluid film damping coefficients.

The values of direct damping coefficients observed higher than cross-coupled stiffness coefficients and the difference increases with journal eccentricities ratios but there is not much increment compare to stiffness also direct damping coefficients have initial values when the journal is not eccentric that indicates initial damping presented without hydrodynamic action. The values non-dimensional of direct and cross-coupled damping corresponding to journal eccentricity ratios of 0.1, 0.2, 0.3, 0.4, 0.5, and 0.6 are shown in Fig. 7(b) by data strips.

3.2. Effect of journal rotational speed

The effect of journal rotational speed on TPJB fluid film coefficients analyzed by increasing journal rotational speed from 2000 rpm to 16000 rpm (above first critical speed).

The values of non-dimensional fluid film thickness on each pad corresponding to journal rotational speeds of 2500 rpm, 10,000 rpm, and 16,000 rpm were presented in Fig. 8 (a). Fig. 8(b) indicates that non-dimensional fluid film forces decreasing nonlinearly corresponding to increment in journal rotational speeds. Higher and lower fluid film forces observed on pad-1 and pad-3 while they are identical on pad-2 and pad-4. The difference between fluid film forces on pads decreases when the journal rotational speed increases that indicate fluid film forces act close to uniformity at higher journal rpm. The values of fluid film forces on each pad corresponding to journal rotation speeds of 2000, 4000, 10000, and 16,000 rpm mentioned inside Fig. 8 (b).

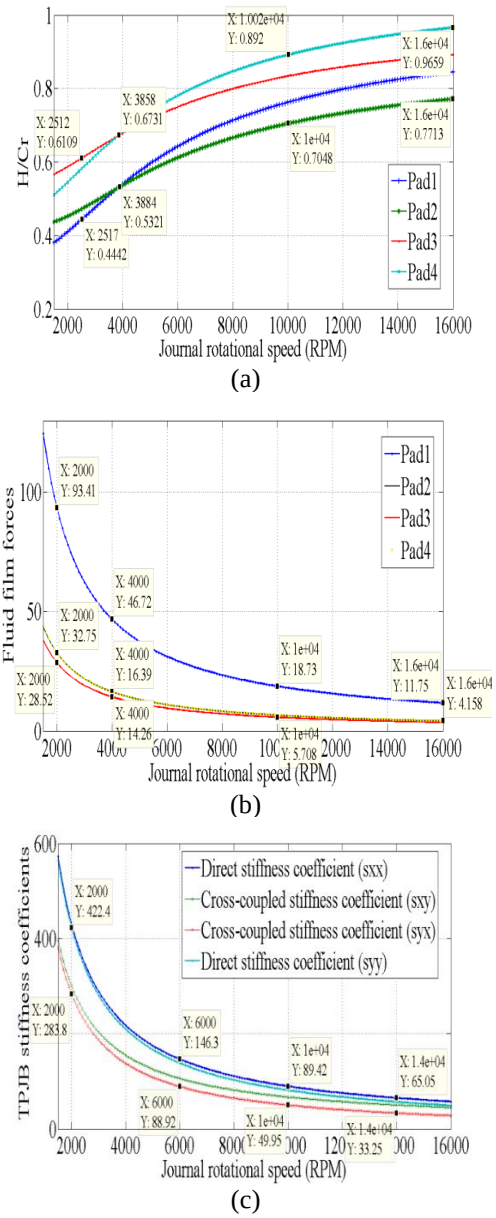

Fig. 8. Change in fluid film properties corresponding to journal rotational speeds, (a) non-dimensional fluid film thickness on pads, (b) non-dimensional fluid film forces on pads, (c) TPJB non-dimensional fluid film stiffness coefficients.

Fig. 8(c) indicates higher values direct of radial stiffness coefficients than cross-coupled stiffness coefficients. The difference between them decreases when journal rotation speed increases. It is also observed that cross-coupled stiffness coefficients play a much significant role at higher rotation speeds particularly when journal speed is above 8000 rpm. The values of non-dimensional fluid film stiffness coefficients of TPJB corresponding to journal rotational speeds of 2000 rpm, 6000 rpm, 10000 rpm, and 14000 rpm are demonstrated inside Fig. 8(c) with the help of data strips.

3.3. Effect of radial clearance

The effect of TPJB radial clearance on TPJB fluid film coefficients analyzed by increasing bearing radial clearance from 50 microns to 150 microns. Fig. 9(a) indicates that non-dimensional fluid film thickness on each pad increases corresponding to bearing radial clearance. The highest non-dimensional fluid film thickness observed on pad-3 in the range of 0.55 to 0.64 while lowest non-dimensional fluid film thickness observed on pad-1 in the range of 0.36 to 0.48. The difference of film thickness between pad-2 and pad-4 increases corresponding to radial clearance while the difference of film thickness between pad-1 and pad-3 remains identical (minor reduction). The values of non-dimensional fluid film thickness on each pad corresponding to TPJB radial clearance of 50 microns, 80 microns, 100 microns, 120 microns, and 150 microns were presented in Fig. 9(a).

Fig. 9(b) indicates that non-dimensional fluid film forces on each pad decreasing nonlinearly corresponding to increment in TPJB radial clearance shows an agreement with previous research [21]. Higher and lower fluid film forces observed on pad-1 and pad-3 while they are identical on pad-2 and pad-4. The difference between fluid film forces on pads decreases when TPJB radial clearance increases that indicate higher clearances cause less supportive fluid film forces hence reduce bearing performance. To provide optimum clearance different parameters i.e. rotation of pad and pad preload is consider during the manufacturing of TPJB. The values of fluid film forces on each pad corresponding to TPJB radial clearance of 50 microns, 80 microns, 100 microns, 120 microns, and 150 microns were presented in Fig. 9(b). Fig. 9(c) indicates higher values direct of radial stiffness coefficients than cross-coupled stiffness coefficients when radial clearance is less than 100 microns. When clearance is 106 microns, the value of the non-dimensional direct stiffness coefficient (s_{yy}) becomes identical to the non-dimensional cross-coupled stiffness coefficient (s_{xy}). When radial clearance is higher

than 106 microns, cross-coupled stiffness coefficient (s_{xy}) becomes the dominant cause's instability in TPJB. The values of non-dimensional fluid film stiffness coefficients of TPJB corresponding to TPJB radial clearances of 50 microns, 80 microns, 100 microns, 120 microns, and 150 microns were presented in Fig. 9(c).

3.4. Effect of slenderness (L/D) ratio

In the presented research, bearing the slenderness ratio was changed from 0 to 1, because the infinitely short bearing assumption was accurate for small slenderness ratios [30]. Fig. 10(a) indicates that there are no fluid film forces when L/D=0 is, i.e. bearing length is 0. Oil film forces increase on all pads non-linearly with increment in slenderness ratio. The maximum value of the fluid film force observed at L/D=1. There is the smaller increment in forces on pad-3 observed than pad-1, pad-2, and pad-4 which may happen due to the position of journal inside TPJB, pad-3 remains unloaded. When the slenderness ratio was higher than 0.5, the slope of the curve increases rapidly, which indicates larger hydrodynamic forces develop on pads.
The values of dimensional fluid film forces on each pad corresponding to TPJB slenderness ratios of 0.2, 0.4, 0.6, 0.8, and 1 were presented in Fig. 10(a). Fig. 10(b) indicates that when the slenderness ratio is smaller than 0.2, the values of direct and cross-coupled stiffness coefficients are less. The magnitude of direct stiffness coefficients, as well as cross-coupled stiffness coefficients, increases rapidly when slenderness ratio is higher than 0.4, also the difference between direct and cross-coupled stiffness coefficients increases when the slenderness ratio increases. The maximum value of direct stiffness (S_{xx}) and cross-coupled stiffness (S_{xy}) observed when the slenderness ratio is unity. Here the point to be noted that high values cross-coupled stiffness coefficient (S_{xy}) induced instability in the system. The values of dimensional fluid film stiffness coefficients of TPJB corresponding to slenderness ratios of 0, 0.2, 0.4, 0.6, 0.8, and 1 were presented in Fig. 10(b). Fig. 10(c) indicates that when the slenderness ratio is smaller than 0.2, the values of direct and cross-coupled damping coefficients are less. The magnitude of direct damping coefficients, as well as cross-coupled damping coefficients, increases rapidly when slenderness ratio is higher than 0.2, also the difference between direct and cross-coupled stiffness coefficients increases when the slenderness ratio increases. The maximum value of direct damping coefficient and cross-coupled damping coefficient was observed when the slenderness ratio is unity.

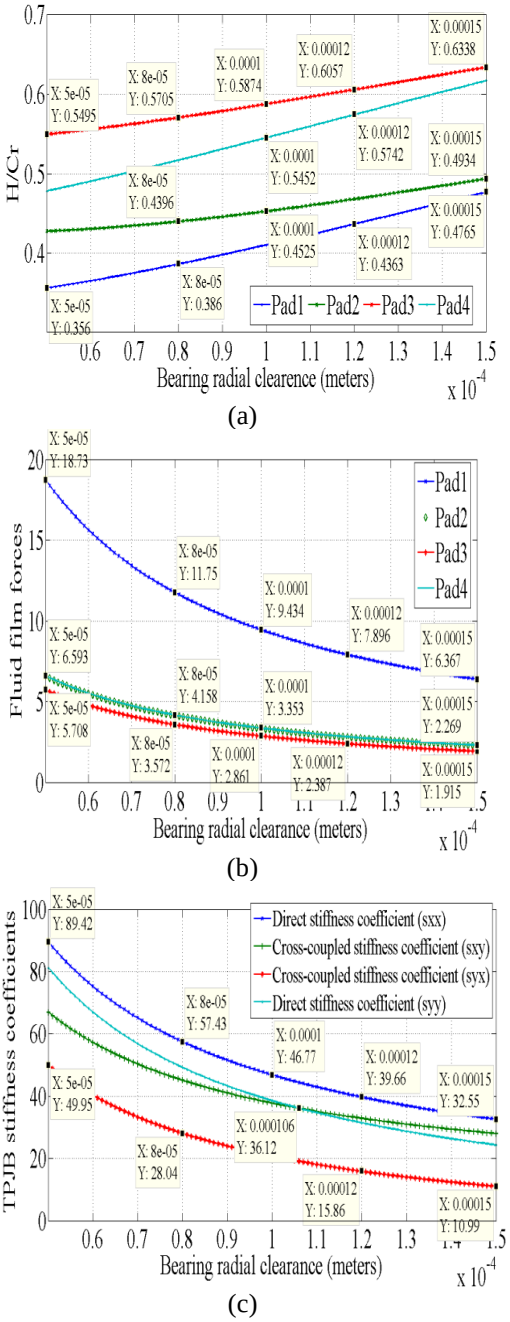

Fig. 9. Change in fluid film properties corresponding to TPJB radial clearance, (a) non-dimensional fluid film thickness on pads, (b) non-dimensional fluid film forces on pads, (c) TPJB non-dimensional fluid film stiffness coefficients.

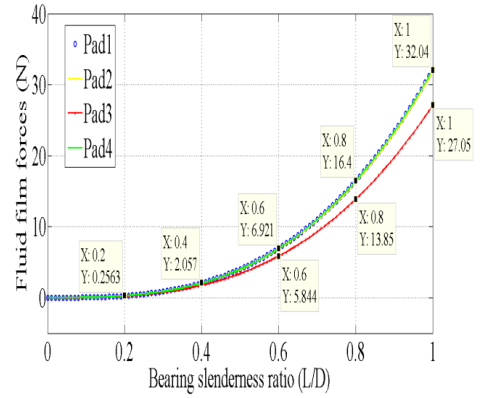

(a)

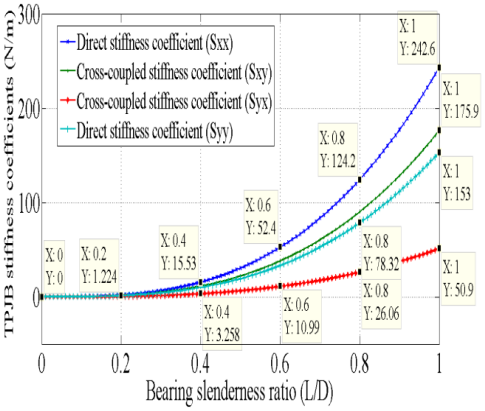

(b)

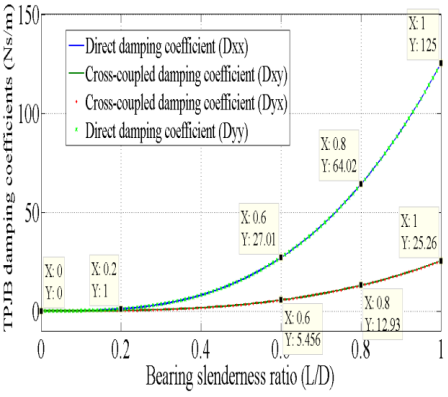

(c)

Fig. 10. Change in fluid film properties corresponding to slenderness ratio of TPJB, (a) dimensional fluid film forces on pads, (b) TPJB dimensional fluid film stiffness coefficients, (c) TPJB dimensional fluid film damping coefficients.

The maximum cross-coupled damping coefficient was observed 20% of the maximum direct damping coefficient. The values of dimensional fluid film damping coefficients of TPJB corresponding to slenderness ratios of 0, 0.2, 0.6, 0.8, and 1 were presented in Fig. 10(c).

3.5. Effect of pad pivot offset

The pad pivot offset is the location of the pivot as a percentage of the pad arc length on a journal tilt pad. The pivot offset has measured from the leading edge of the pad. A center-pivot termed as 50% of the pad arc length. A typical "offset pivot" might be at 60% to get optimum fluid film convergence. The pad pivot offset calculated as $\alpha_p = \frac{\phi_0}{\chi_p}$, here ϕ_0 is pivot angle from the leading edge from pad and χ_p is pad arc angle. When pivot offset is 0.35, pad-3 and pad-4 have identical fluid film thickness. When the pivot offset is greater than 0.35, the highest fluid film thickness observed on pad-3 while lowest fluid film thickness observed on pad-4. The fluid film thickness on pad-2 and pad-4 also observed identical when pad pivot offset is 0.58. Higher fluid film thickness observed when pivot offset was less than 50 present which shows an agreement with previous research [21]. The values of non-dimensional fluid film thickness on each pad corresponding to pad pivot offset on each pad of 0, 0.2, 0.5, and 1 were presented in Fig. 11(a). Fig. 11(b) indicates a nonlinear increment of fluid film forces on pad-1 which is showing agreement with previous research [21] and nonlinear decrement of the same on the pad-3 corresponding to increment in pad pivot offset. When pad pivot offset is 0.37, fluid film forces on pad-1 and pad-2 have identical values also when pad pivot offset is 0.46; fluid film forces on pad-1 and pad-4 have identical values. When pad pivot offset is lower than 0.46, highest fluid film forces observed on pad-4 while lowest fluid film forces observed on pad-3 also when it is higher than 0.46, highest fluid film forces observed on pad-1 and lowest fluid film forces observed on pad-3. The values of dimensional fluid film forces on each pad corresponding to pad pivot offset on each pad of 0, 0.5, 0.5, and 1 was presented in Fig. 11(b). Fig. 11(c) indicates direct stiffness as well as cross-coupled stiffness of TPJB increases nonlinearly with pivot offset but as the slope of the curve is found less, the rate of increment is less. The direct stiffness coefficients (S_{xx}) have a maximum range of values while cross-coupled stiffness coefficients (S_{yx}) have a minimum range of values corresponding to increment in pad pivot offset. but when α_p is greater than 0.6, cross-coupled stiffness is almost constant but they have a large

difference. The values of dimensional fluid film stiffness coefficients of TPJB corresponding to pad pivot offset of 0, 0.2, 0.4, 0.5, 0.8, and 1 was presented in Fig. 11(c).

3.6. Effect of number of pads

The number of pads may vary according to the desired response in TPJB. Table 3 represents pad angles, leading-edge angles, trailing edge angles, pad pivot angles, and the gap between pads in TPJB. These geometrical parameters may change according to the functioning requirement of the system. The numbers of pads for analysis were varying from 2 to 11. Fig. 12 represents the change in fluid film forces corresponding to non-dimensional journal eccentricities for the different number of pads inside TPJB.

For the same eccentricity ratio, dimensional fluid film forces decrease when the number of pads increases. That is due to the lesser surface area of the pad was available to develop fluid film forces. There are some exceptional cases i.e. when the number of pads was 4 and 8 where fluid film forces were found smaller than their expected values. The values of maximum and minimum net dimensional fluid film forces of TPJB corresponding to non-dimensional journal eccentricities of 0, 0.2, 0.3,0.4,0.5, and 0.6 for the different number of pads in TPJB was presented in Fig. 12. Fig. 13(a) represents the change in direct stiffness coefficients (S_{xx}) corresponding to non-dimensional journal eccentricities for the different number of pads. The range of values of direct stiffness coefficients (S_{xx}) decreases when the number of pads increases. There are some exceptional cases i.e. when the number of pads was 4, 6 where values of direct stiffness coefficients (S_{xx}) were found smaller than their expected values. When non-dimensional journal eccentricity is lower than 0.3, the highest values of direct stiffness coefficients (S_{xx}) observed for 8-pads TPJB while the lowest values for the same observed for 4-pads TPJB. When non-dimensional journal eccentricity is higher than 0.3, the highest values of direct stiffness coefficients (S_{xx}) observed for 2-pads TPJB while the lowest value for the same observed for 4-pads TPJB. Fig. 13(b) represents the change in cross-coupled stiffness coefficients (S_{xy}) corresponding to non-dimensional journal eccentricities for the different number of pads.

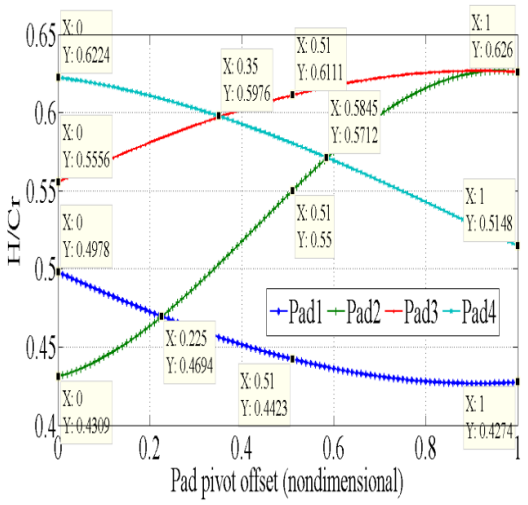

(a)

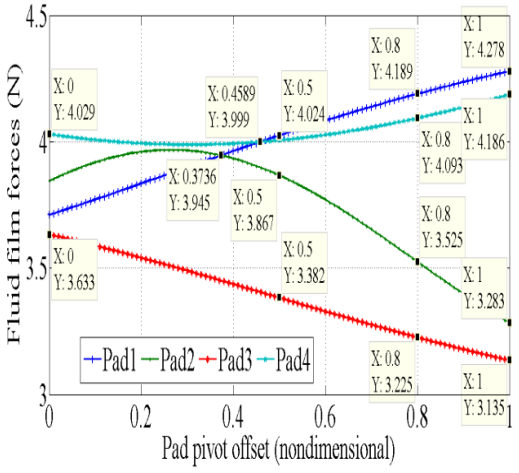

(b)

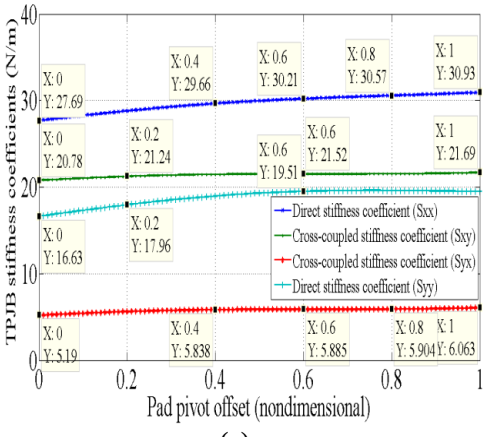

(c)

Fig. 11. Change in fluid film properties corresponding to pad pivot offset, (a) non-dimensional fluid film thickness on pads, (b) dimensional fluid film forces on pads, (c) TPJB dimensional fluid film stiffness coefficients.

The range of values of cross-coupled stiffness coefficients (S_{xy}) decreases when increases the number of pads.

There are some exceptional cases i.e. when the number of pads was 4, 6 where values of cross-coupled stiffness coefficients (S_{xy}) were found smaller than their expected values. The highest values of cross-coupled stiffness coefficients (S_{xy}) observed for 2-pads TPJB while the lowest values for the same observed for 4-pads TPJB. Fig. 14(a) represents the change in direct damping coefficients (D_{xx}) corresponding to non-dimensional journal eccentricities for the different number of pads. The range of values of direct damping coefficients (D_{xx}) decreases when it increases the number of pads.

There is an exceptional case i. e. when the number of pads was 4 where a value of direct damping coefficients (D_{xx}) was found smaller than its expected values within the range of journal eccentricity ratios. When journal eccentricity is lower than 0.36, the highest values of direct damping coefficients (D_{xx}) observed for 2-pads TPJB while the lowest values for the same observed for 12-pads TPJB. When non-dimensional journal eccentricity is higher than 0.36, the highest values of direct damping coefficients (D_{xx}) observed for 2-pads TPJB while the lowest value for the same observed for 4-pads TPJB. Fig. 14 (b) represents the change in cross-coupled damping coefficients (D_{xy}) corresponding to journal eccentricity ratios for the different number of pads. The range of values of cross-coupled damping coefficients (D_{xy}) decreases when it increases the number of pads.

There are some exceptional cases i.e. when the number of pads was 4, 5, and 6 where values of cross-coupled damping coefficients (D_{xy}) were found smaller than their expected values. When journal eccentricity ratio is lower than 0.53, highest values of cross-coupled damping coefficients (D_{xy}) observed for 8-pads TPJB while lowest values for same observed for 4-pads TPJB also when journal eccentricity ration is greater than 0.53, highest values of cross-coupled damping coefficients (D_{xy}) observed for 3-pads TPJB while lowest values for same observed for 4-pads TPJB.

Table 3. TPJB pad angles related to the numbers of pads.

No of pads	Pad arc angle (°)	The angular gap between pads (°)	Pad leading angle (Φ_l°)	Pad trailing angle (Φ_t°)	Pad pivot location at 50% offset (ϕ_0°)
2	170	10	5	175	90
			185	355	270
3	110	10	5	115	60
			125	235	180
			245	355	300
4	80	10	5	85	45
			95	175	135
			185	265	225
			275	355	315
5	62	10	5	67	36
			77	139	108
			149	211	180
			221	283	252
			293	355	324
6	50	10	5	55	30
			65	115	90
			125	175	150
			185	235	210
			245	295	270
			305	355	330
8	35	10	5	40	22.5
			50	85	67.5
			95	130	112.5
			140	175	157.5
			185	220	202.5
			230	265	247.5
			275	310	292.5
			320	355	337.5
9	30	10	5	35	20
			45	75	60
			85	115	100
			125	155	140
			165	195	180
			205	235	220
			245	275	260
			285	315	300
			325	355	340
10	26	10	5	31	18
			41	67	54
			77	103	90
			113	139	126
			149	175	162
			185	211	198
			221	247	234
			257	283	270
			293	319	306
			329	355	342
12	20	10	5	25	15
			35	55	45
			65	85	75
			95	115	105
			125	145	135
			155	175	165
			185	205	195
			215	235	225
			245	265	255
			275	295	285
			305	325	315
			335	355	345

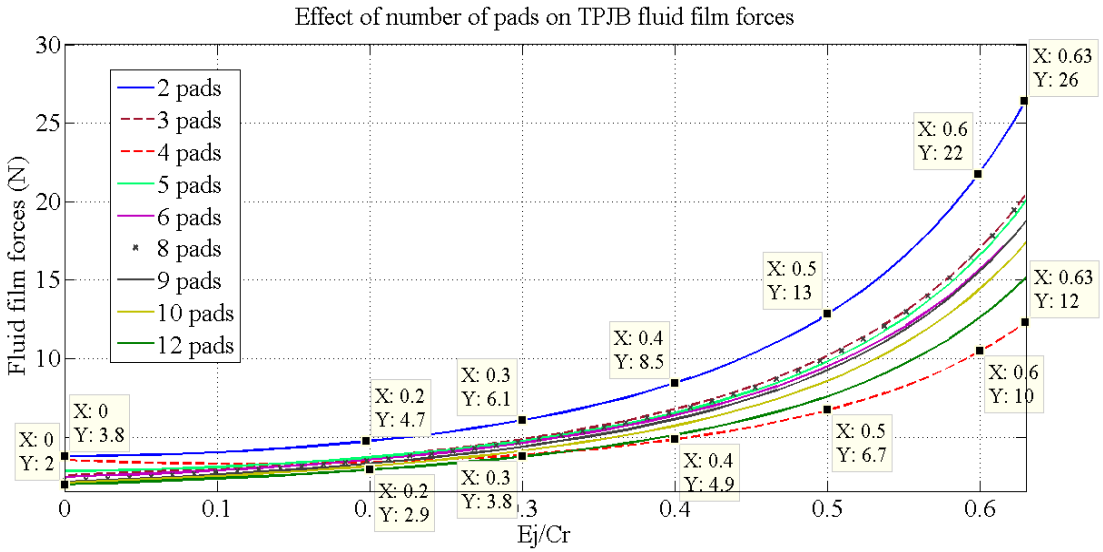

Fig. 12. Change in TPJB dimensional fluid film forces corresponding to journal eccentricity ratios for the different number of pads.

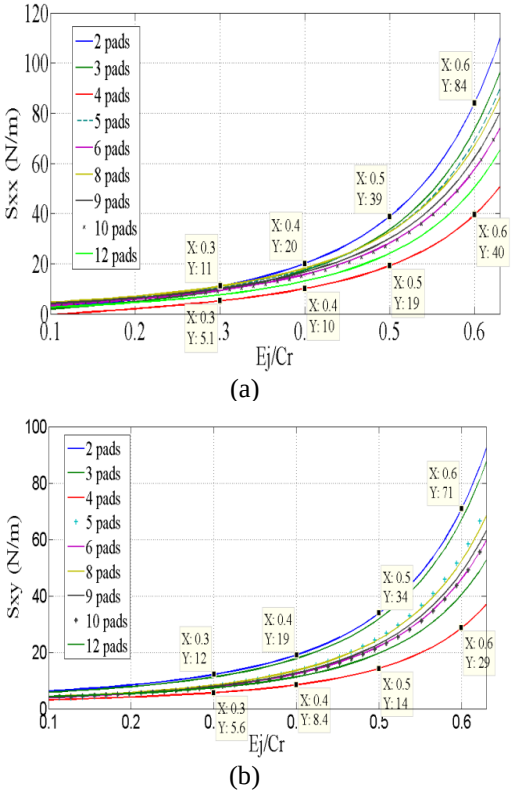

(a)

(b)

Fig. 13. Change in TPJB dimensional stiffness coefficients corresponding to non-dimensional journal eccentricities for the different number of pads, (a) Direct stiffness coefficients (S_{xx}) for the different number of pads, (b) Cross-coupled stiffness coefficients (S_{xy}) for the different number of pads.

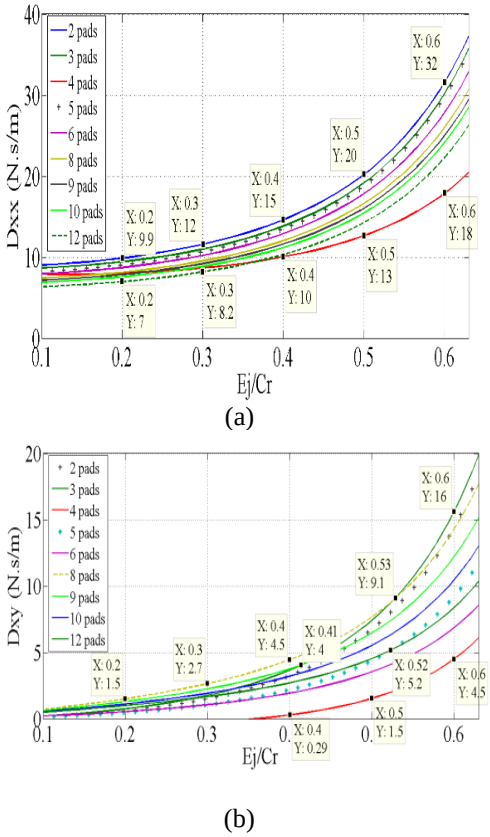

(a)

(b)

Fig. 14. Change in TPJB dimensional damping coefficients corresponding to non-dimensional journal eccentricities for the different number of pads, (a) Direct damping coefficients (D_{xx}) for the different number of pads, (b) Cross-coupled damping coefficients (D_{xy}) for the different number of pads.

4. Conclusions

The modified analytical approach presented to analyze effects of journal eccentricity, journal rotational speed, radial clearance, slenderness ratio, pad pivot offset, and the number of pads on fluid film thickness, fluid film forces, fluid film moments and fluid film stiffness and damping coefficients on each pad and whole TPJB. Indigenous Matlab™ code has been developed for analysis purposes. Results produced in the form of design curves comparing changes in fluid film properties corresponding to TPJB geometric parameters. Pressure and forces obtained by the proposed analytical method show agreement with methods adopted in previous researches to prove the novelty of the proposed method. For accuracy measurement, error analysis is performed on validation plots and variations in errors represented in the form of error bars. Comparative analysis has conducted to find the effect of geometric parameters of TPJB on fluid film properties. This research is useful and applicable for other research because the results not only provide sufficient sources of data regarding the change in properties of the fluid film corresponding to geometrical parameters by design curves but also the designer can use those charts to determine appropriate values geometrical parameters to satisfy operation requirement of TPJB.

From the analysis of the above-mentioned figures the following points have been concluded:

- The values of non-dimensional fluid film thickness will always less than unity to ensure that the journal remains inside bearing.
- Large journal eccentricity ratio cause decrement in fluid film thickness, that provides higher fluid film forces but minimum fluid film thickness should be maintained to prevent interaction or direct contact between journal and pads.
- Fluid film thickness also depends on the location of the journal inside the TPJB; the location of the journal insists on the loading and unloading of pads.
- Large journal eccentricity ratios lead to high fluid film stiffness and damping coefficients but in that case, cross-coupled stiffness and damping coefficients also increase and cause instability in TPJB. Although the values of cross-coupled stiffness and damping are less as compare to direct stiffness and damping coefficients yet at higher eccentricities, these values are significant.
- Increment in journal rotational speed causes an increment in fluid film thickness, which causing lesser fluid film forces. The amount of decrement in fluid film forces are more on loaded pads than on unloaded pads.
- Increment in journal rotational speeds leads to a reduction in direct and cross-coupled fluid film stiffness coefficients. Cross-coupled stiffness coefficients are not imparting much influence of the stability of TPJB as they remain lower than direct ones at higher journal rotational speeds.
- Increment in bearing radial clearance causes an increment in fluid film thickness on all pads that causing lesser fluid film forces, which shows an agreement with previous research [21]. The reduction in fluid film forces is more in loaded pads than corresponding to unloaded pads.
- Increased bearing radial clearance leads to a reduction in fluid film stiffness coefficients, cross-coupled stiffness provides significant effect when bearing radial clearance is higher than 50% of assembling clearance causing instability in TPJB.
- Higher slenderness ratio causes an increment in fluid film forces, the values of fluid film forces increase rapidly when the slenderness ratio is higher than 0.4. The fluid film forces on unloaded pad have lesser values than the same on loaded pads.
- Higher slenderness ratio leads to larger fluid film stiffness and damping coefficients. Cross-coupled stiffness and damping coefficients also increasing with slenderness ratio causing instability in TPJB. The values of cross-coupled stiffness coefficients become much significant at a higher slenderness ratio. The direct damping coefficients are higher than cross-coupled damping coefficients and difference increases at higher slenderness ratios, which provide sufficient stability in TPJB.
- Increment in fluid film thickness observed on unloaded pads (pad-2 and pad-3) while decrementing in fluid film thickness observed on the unloaded pad (pad-1 and pad-4), that provide larger fluid film forces on loaded pads and smaller fluid film forces on unloaded pads with

increment in pad pivot offset. That results showing an agreement with previous research [21]. Larger minimum fluid film thickness obtained when pad pivot offset is within 0.5.

- The pad pivot offset does not affect much on direct and cross-coupled fluid film stiffness coefficients except the larger rate of increment in stiffness coefficients observed on loaded pads than unloaded pads also to decide the value of pad pivot offset designer should consider minimization of cross-coupled stiffness coefficients as they play an important role in TPJB stability.
- Hydrodynamic fluid film forces decrease when the number of pads in TPJB increases but there were some exceptions.
- Minimum values of direct and cross-coupled stiffness coefficients observed when TPJB has 4 numbers of pads that indicate that 4-pad TPJB is acting uniformly at low load conditions.
- For the same eccentricity ratios values of direct stiffness coefficients have much larger values than its corresponding cross-coupled stiffness coefficients showing agreement with previous research [14]. That indicates that although direct stiffness coefficients have larger values cross-coupled stiffness coefficients also play a significant role in the stability of TPJB.
- Minimum values of direct and cross-coupled damping coefficients observed when TPJB has 4 numbers of pads when the journal eccentricity ratios are higher than 0.45 that indicates in the operating conditions, 4-pad TPJB provides much lesser damping than other configurations also it provides uniform displacement of the journal at the horizontal and vertical direction which is showing agreement with previous research [21].
- For the same eccentricity ratios values of direct damping coefficients have much larger values than its corresponding cross-coupled damping coefficients. That indicates that although higher values of direct damping coefficients provide higher stability to the system yet small values of cross-coupled damping coefficients also influence the stability of the system particularly when the journal operates at higher eccentricities.

The response of the system supported by TPJB depends on the combination of all geometrical parameters so it is a tedious process to identify the effect of a single parameter, so in this research to analyze the effect of a single parameter on fluid film properties, the constant value provided for other parameters. This research is applicable to understand insides of TPJB also it is useful to select applicable values of geometrical parameters to design TPJB according to its operating requirement, also this research provides applicable data related to fluid film properties for coding related problems to get the dynamic response of the system supported by TPJB.

Compliance with ethical standards

Conflict of Interest The authors declare that they have no conflict of interest.

References

[1] D. Timothy, A. Younan, and P. Allaire, "A review of tilting pad bearing theory." *Int. J. Rotating Mach.*, Vol. 2011, pp. 1-23, (2011).

[2] A. Ghasem, M. Adnan, and D. W. Childs, "Rotordynamic coefficients measurements versus predictions for a high-speed flexure-pivot tilting-pad bearing (load-between-pad configuration)" *J. Eng. Gas Turbines Power*, Vol. 128, No. 4, pp. 896-906, (2006).

[3] E. P. Okabe, "Analytical model of a tilting pad bearing including turbulence and fluid inertia effects." *Tribol. Int.*, Vol. 114, pp. 245-256, (2017).

[4] J. W. Lund, "Spring and damping coefficients for the tilting-pad journal bearing." *ASLE transactions.*, Vol. 7, No. 4, pp.342-352, (1964).

[5] J. C. Nicholas and R. G. Kirk, "Four pad tilting pad bearing design and application for multistage axial compressors." *J. Tribol. Tech.*, Vol. 104, No. 4, pp. 523-529, (1982).

[6] M. F. White, E. Torbergsen and V. A. Lumpkin, "Rotordynamic analysis of a vertical pump with tilting-pad journal bearings." *Wear*, Vol. 207, No. 1-2, pp. 128-136, (1997).

[7] F. Feng and F. Chu, "Influence of pre-load coefficient of TPJBs on shaft lateral

vibration." *Tribol. Int.*, Vol. 35, No. 1, pp. 65-71, (2002).

[8] I. A. Mahfouz and M. L. Adams, "Numerical study of some nonlinear dynamics of a rotor supported on a three-pad tilting pad journal bearing (TPJB)." *J. Vib. Acoust.*, Vol. 127, No. 3, pp. 262-272, (2005).

[9] E. P. Okabe and K. L. Cavalca, "Rotordynamic analysis of systems with a non-linear model of tilting pad bearings including turbulence effects." *Nonlinear Dyn.*, Vol. 57, No. 4, pp. 481-495, (2009).

[10] E. P. Okabe, "Analytical model of a tilting pad bearing including turbulence and fluid inertia effects." *Tribol. Int.*, Vol. 114, pp. 245-256, (2017).

[11] J. Luneno, J. Aidanpaa, and R. Gustavsson, "Misalignment in combi-bearing: A cause of parametric instability in vertical rotor systems." *J. Eng. Gas Turbines Power* Vol. 135, No. 3, 032501, (2013).

[12] J. Luneno, J. Aidanpaa and R. Gustavsson, "Experimental verification of a combi-bearing model for vertical rotor systems." *J. Vib. Acoust.*, Vol. 135, No. 3, 034501, (2013).

[13] M. Nasselqvist, R. Gustavsson and J. Aidanpaa, "Experimental and numerical simulation of unbalance response in vertical test rig with tilting-pad bearings." *Int. J. Rotating Mach.*, Vol. 2014, pp. 1-10, (2014).

[14] E. Synnegard, R. Gustavsson and J. Aidanpaa, "Influence of cross-coupling stiffness in tilting pad journal bearings for vertical machines." *Int. J. Mech. Sci.*, Vol. 111-112, pp. 43-54, (2016).

[15] E. Synnegard, R. Gustavsson and J. Aidanpaa, "Forced response of a vertical rotor with tilting pad bearings." *In 16th Int. Symposium on Transport Phenomena and Dynamics of Rotating Machinery*, Vol. 1, No. 1, pp. 1-8, (2016).

[16] E. Khosravian and S. Ghatreh. "Dynamic Properties of Tilting-Pad Journal Bearings in Power Plant Iran (Yazd Station)." *Indian J. Sci. Res.*, Vol. 1, No. 2, pp. 690-701, (2014).

[17] A. Chasalevris, "Analytical evaluation of the static and dynamic characteristics of three-lobe journal bearings with finite length." *J. Tribol.*, Vol. 137, No. 4, pp. 041701(01-16), (2015).

[18] P. Sharabiani, Pouya and H. Ahmadian, "Nonlinear model identification of oil-lubricated tilting pad bearings." *Tribol. Int.*, Vol. 92, pp. 533-543, (2015).

[19] P. Dang, S. Chatterton, P. Pennacchi, A. Vania, and F. Cangioli, "Investigation of load direction on a five-pad tilting pad journal bearing with variable clearance." *In Proceedings of the 14th IFToMM World Congress*, pp. 503-511, (2015).

[20] Y. Jin, Z. Shi, X. Zhang and X. Yuan, "Rapid solution for analysis of nonlinear fluid film force and dynamic behavior of a tilting-pad journal bearing-rotor system with turbulent and thermal effects." *Frict.*, Vol. 8, No. 2, pp. 343-359, (2020).

[21] Y. Jin, F. Chen, J. Xu, and X. Yuan, "Nonlinear dynamic analysis of low viscosity fluid-lubricated tilting-pad journal bearing for different design parameters." *Frict.*, Vol. 8, No. 5, pp. 930-944, (2020).

[22] E. Ciulli, P. Forte, M. Libraschi, L. Naldi, and M. Nuti, "Characterization of high-power turbomachinery tilting pad journal bearings: First results obtained on a novel test bench." *Lubr.*, Vol. 6, No. 4, pp. 1-15, (2018).

[23] E. Ciulli, and P. Forte, "Nonlinear Response of Tilting Pad Journal Bearings to Harmonic Excitation." *Mach.*, Vol. 7, No. 43, p. 1-14, (2019).

[24] H. Silva and R. Nicoletti, "Design of tilting-pad journal bearings considering bearing clearance uncertainty and reliability analysis." *J. Tribol.*, Vol. 141, No. 1, pp. 1-26, (2019).

[25] L. Andres, B. Koo and M. Hemmi, "A flow starvation model for tilting pad journal bearings and evaluation of frequency response functions: a contribution towards understanding the onset of low frequency shaft motions." In *ASME Turbo Expo 2017:*

Turbomachinery Technical Conference and Exposition. *ASME Digital Collection*, Vol. 140, No. 1, pp. 052506 (1-14), (2017).

[26] M. Barsanti, E. Ciulli, P. Forte, M. Libraschi and M. Strambi. "Error analysis in the determination of the dynamic coefficients of tilting pad journal bearings." *Procedia Struct. Integrity*, Vol. 24, No. 1, pp. 988-996, (2019).

[27] M. Barsanti, E. Ciulli and P. Forte, "Random error propagation and uncertainty analysis in the dynamic characterization of Tilting Pad Journal Bearings." *J. Phys. Conf. Ser.*, Vol. 1264, No. 1, pp. 012035(1-11), (2019).

[28] L. R. Ito, D. J. Ramos, Z. de C. Silveira, and G. B. Daniel. "Parametric Sensitivity Analysis of Tilting Pad Bearings to Investigate the Dynamic Behavior of Rotating Machines, " *Int. Conf. Rotor Dyn.*, Vol. 1, No. 1, pp. 292-306, (2018).

[29] I. F. Santos and F. H. Russo, "Tilting-pad journal bearings with electronic radial oil injection." *J. Tribol.*, Vol. 120, No. 3, pp. 583-594, (1998).

[30] J. S. Rao, "*Rotor dynamics", New Age International*, pp. 161-196, (1996).

[31] Y. Wang, Y. Gao, Y. Cui and Z. Liu, "Establishment of approximate analytical model of oil film force for finite length tilting pad journal bearings." *Int. J. Rotating Mach.*, Vol. 1, No. 1, pp. 1-11, (2015).

[32] Y. J. Lu, L. F. Ji, Y. F. Zhang, Y. Wu, Y. Y. Liu and L. Yu, "Dynamic behaviours of the rotor non-linear system with fixed—tilting-pad journal bearings support." *Proc. Inst. Mech. Eng., Part J: J. Eng. Tribol.*, Vol. 224, No. 10, pp. 1037-1047, (2010).

How to cite this paper:

Harsh Kumar Dixit and T. C. Gupta, "Effect of geometrical parameters on fluid film coefficients in tilting pad journal bearing", *J. Comput. Appl. Res. Mech. Eng.*, Vol. 10, No. 2, pp. 405-426, (2021).

DOI: 10.22061/jcarme.2020.5453.1679

URL: https://jcarme.sru.ac.ir/?_action=showPDF&article=1263